Supplementary Information(SI)

Single-, double-, and triple-atom catalysts on graphene-like C₂N enable electrocatalytic nitrogen reduction: insight from first principles

Jin Zhang, Wei An*

College of Chemistry and Chemical Engineering, Shanghai University of Engineering Science, 333 Longteng Road, Songjiang District, Shanghai 201620, China

*E-mail: weian@sues.edu.cn

Table S1. Zero-point energy (ZPE, eV) and entropy correction (TS, eV) at T = 298 K for adsorbates on $Ni_2@C_2N$.

Configuration	adsorbate	ZPE/(eV)	TS/(eV)
	*N_2	0.19	0.13
	*NNH	0.52	0.09
	*NHNH	0.83	0.11
Enzymatic	*$NHNH_2$	1.19	0.11
	*NH_2NH_2	1.49	0.11
	* NH_2	0.72	0.06
	* NH_3	1.04	0.13

Table S2. The $M_3@C_2N$ three possible configurations and their corresponding binding energy (*BE*, in eV)[1]. The gray, blue, and green spheres represent C, N, and M_3 atoms, respectively. Bold fonts represent the most stable configuration.

$M_3@C_2N$	I	II	III	IV
Cr	**-6.50**	/	-6.02	-5.73
Fe	**-6.74**	/	-5.92	-5.43
Co	**-7.03**	/	-6.01	-5.14
Ni	**-6.93**	/	-5.58	-4.79
Mo	/	**-7.60**	-7.09	-6.45
W	/	**-7.85**	-7.10	-6.04

[1] $BE = E_{M_n@C_2N} - E_{M_n} - E_{C_2N}$, where $E_{M_n@C_2N}$, E_{C_2N} and E_{M_n} are the total energies of $M_n@C_2N$ system, the C_2N monolayer, and the isolated M_n cluster, respectively.

Table S3. DFT-calculated Bader charge transfer (Δq) from M_n to C_2N substrate equivalent to oxidation state of $M_n^{\delta+}$.

	$M_1@C_2N$ $M_1^{\delta+}$	$M_2@C_2N$ $M_1^{\delta+}/M_2^{\delta+}$	$M_3@C_2N$ $M_1^{\delta+}/M_2^{\delta+}/M_3^{\delta+}$
Cr	+1.28	+0.88/+0.88	+0.72/+0.62/+0.79
Fe	+1.11	+0.74/+0.74	+0.60/+0.48/+0.60
Co	+0.85	+0.66/+0.66	+0.46/+0.45/+0.48
Ni	+0.77	+0.57/+0.60	+0.42/+0.41/+0.44
Mo	+1.29	+0.92/+0.91	+0.43/+0.71/+0.96
W	+1.36	+0.98/+0.99	+0.40/+0.77/+1.06

Table S4. DFT-calculated binding energy (BE, eV), Bader charge transfer (Δq, e$^-$)[1], the spin magnetic moment (μ), adsorption energy (E_{ads}, eV) and bond length of $*N_2$ (BL, in Å)[2].

| | | M$_n$@C$_2$N | | | *N$_2$/M$_n$@C$_2$N | | | | | | | |
| | | BE | E_c | μ | Δq, e$^-$ | Side-on | | | Δq, e$^-$ | End-on | | |
		slab	M$_n$	M$_n$ cluster	*N$_2$	E_{ads}	BL	μ	N$_2$	E_{ads}	BL	μ
M$_1$	Cr	-4.36	-4.02	6.0	/	/	/	/	0.22	-0.26	1.12	2.0
	Fe	-4.38	-4.90	4.0	0.31	-0.22	1.15	4.0	0.24	-0.76	1.13	2.0
	Co	-4.25	-5.14	3.0	0.32	-0.34	1.16	1.0	0.25	-0.93	1.13	1.0
	Ni	-4.91	-4.89	2.0	0.26	-0.09	1.15	0.0	0.19	-0.58	1.13	1.0
	Mo	-5.14	-6.31	6.0	0.46	-0.31	1.18	2.0	0.37	-0.85	1.15	2.0
	W	-5.94	-8.38	6.0	0.57	-0.65	1.20	2.0	0.42	-1.10	1.15	2.0
M$_2$	Cr	-5.99	-4.19	4.0	0.74	-1.65	1.20	0.0	0.36	-1.07	1.14	2.0
	Fe	-5.66	-3.59	6.0	0.54	-0.84	1.17	2.0	0.33	-0.85	1.14	2.0
	Co	-5.50	-3.67	4.0	0.47	-0.68	1.17	0.0	0.37	-1.07	1.15	0.0
	Ni	-5.71	-3.34	2.0	0.39	-0.15	1.17	2.0	0.35	-0.49	1.15	2.0
	Mo	-6.72	-4.36	0.0	0.66	-0.33	1.22	0.0	0.33	-0.87	1.14	2.0
	W	-8.65	-6.01	0.0	1.06	-0.81	1.29	0.0	0.35	-0.89	1.14	0.0
M$_3$	Cr	-6.50	-3.17	6.0	1.24	-1.93	1.31	4.0	0.55	-1.33	1.16	2.0
	Fe	-6.74	-3.15	10.0	0.92	-1.55	1.26	6.0	0.48	-1.01	1.16	6.0
	Co	-7.03	-3.33	6.5	0.85	-1.34	1.26	3.0	0.32	-1.19	1.16	1.2
	Ni	-6.93	-2.93	2.0	0.62	-0.87	1.22	0.0	0.46	-1.27	1.16	0.0
	Mo	-7.60	-4.20	2.0	0.73	-1.36	1.20	0.0	0.34	-1.11	1.14	0.0
	W	-7.85	-4.94	2.0	0.89	-1.51	1.23	0.0	0.31	-1.17	1.14	0.0

[1]Positive values denote partial charge gained by $*N_2$.

[2]Calculated BL for gaseous N_2 is 1.115 Å.

Table S5. DFT-calculated dissolution potential (U_{dis})[1] of M$_n$ in C$_2$N.

	U_M^0	n	M$_1$ U_{dis}	M$_2$ U_{dis}	M$_3$ U_{dis}
Cr	-0.91	2	-0.74	-1.87	-1.63
Fe	-0.45	2	-0.71	-0.95	-1.05
Co	-0.28	2	-0.72	-0.76	-0.84
Ni	-0.26	2	-0.48	-0.52	-0.71
Mo	-0.20	3	-0.59	-0.48	-1.19
W	0.10	3	-0.71	-0.21	-1.10

[1]$U_{dis} = U_M^0 + [\mu_{M,bulk} - (E_{M_n@C_2N} - E_{M_{n-1}@C_2N})]/ne$, where U_M^0 is standard dissolution potential of M in bulk form.

Table S6. DFT-calculated oxidation state of M_n as a result of side-on $*N_2$ adsorption on $M_n@C_2N$.

	$M_1@C_2N$ $M_1^{\delta+}$	$M_2@C_2N$ $M_1^{\delta+}/M_2^{\delta+}$	$M_3@C_2N$ $M_1^{\delta+}/M_2^{\delta+}/M_3^{\delta+}$
Cr	/	+1.20/+1.18	+0.96/+1.02/+1.12
Fe	+1.14	+0.95/+0.90	+0.81/+0.83/+0.83
Co	+0.95	+0.83/+0.79	+0.69/+0.70/+0.71
Ni	+0.78	+0.68/+0.66	+0.58/+0.60/+0.63
Mo	+1.51	+1.24/+1.17	+0.80/+1.06/+1.04
W	+1.65	+1.54/+1.59	+0.83/+1.20/+1.13

Table S7. The adsorption energy (E_{ads}) of $*N_2$, $*N_2H$, $*NH_2$ and $*NH_3$ of the two adsorption configurations.

		Side-on		End-on		Side-on/End-on	
		$E_{ads}(*N_2)$	$E_{ads}(*N_2H)$	$E_{ads}(*N_2)$	$E_{ads}(*N_2H)$	$E_{ads}(*NH_2)$	$E_{ads}(*NH_3)$
M_1	Cr	/	/	-0.26	-1.51	-2.71	-1.17
	Fe	-0.22	-1.38	-0.76	-1.72	-2.71	-1.25
	Co	-0.34	-1.61	-0.93	-1.92	-2.51	-1.31
	Ni	-0.09	-1.47	-0.58	-1.62	-2.19	-1.19
	Mo	-0.31	-2.05	-0.85	-2.68	-3.25	-1.04
	W	-0.65	-2.69	-1.10	-3.12	-3.75	-1.42
M_2	Cr	-1.65	-3.82	-1.31	-3.02	-4.39	-1.33
	Fe	-0.84	-2.36	-0.78	-2.58	-3.77	-1.00
	Co	-0.68	-2.35	-1.07	-2.75	-3.81	-1.06
	Ni	-0.15	-2.07	-0.49	-2.37	-3.17	-0.61
	Mo	-0.33	-2.66	-0.87	-2.55	-3.66	-1.16
	W	-0.81	-3.20	-0.89	-2.79	-3.80	-1.20
M_3	Cr	-1.93	-4.14	-1.33	-3.44	-4.67	-1.44
	Fe	-1.55	-3.49	-1.01	-3.22	-4.21	-1.08
	Co	-1.34	-3.56	-1.19	-3.19	-4.10	-1.17
	Ni	-0.87	-3.06	-1.27	-2.83	-3.67	-0.92
	Mo	-1.36	-3.30	-1.11	-3.05	-4.27	-1.49
	W	-1.51	-3.58	-1.17	-3.13	-4.29	-1.58

Table S8. Gibbs free energy change (ΔG, in eV) for the first PCET step ($*N_2 + H^+ + e^- \rightarrow *NNH$) and the last PCET step ($*NH_2 + H^+ + e^- \rightarrow *NH_3$) of the two adsorption configurations as well as desorption of $*NH_3$ with solvation corrections included, at $T = 298.15$ K. The $\Delta G^{de}(*NH_3)$ in italics represent the data above the threshold value $(0.75eV)$[1] that can be regarded as insurmountable for reactions or desorption occurring at room temperature.

		Side-on		End-on		Side-on/End-on		
		$\Delta G(*N_2)$	$\Delta G(*N_2H)$	$\Delta G(*N_2)$	$\Delta G(*N_2H)$	$\Delta G(*NH_3)$	$\Delta G(*H)$	$\Delta G^{de}(*NH_3)$
M_1	Cr	/	/	0.28	0.99	-0.70	0.56	0.67
	Fe	0.26	1.11	-0.16	1.20	-0.80	0.79	*0.79*
	Co	0.14	1.01	-0.40	1.25	-1.05	0.37	*0.82*
	Ni	0.39	0.93	-0.06	1.22	-1.23	0.64	0.70
	Mo	0.21	0.51	-0.30	0.39	-0.10	-0.17	0.57
	W	-0.11	0.21	-0.54	0.20	0.06	-0.53	*0.92*
M_2	Cr	-1.11	0.10	-0.77	0.53	0.66	-0.20	*0.89*
	Fe	-0.29	0.74	-0.23	0.47	0.38	-0.02	0.55
	Co	-0.14	0.61	-0.51	0.59	0.34	-0.18	0.60
	Ni	0.36	0.41	0.03	0.43	0.16	0.03	0.15
	Mo	0.23	-0.17	-0.33	0.57	0.07	-0.11	0.73
	W	-0.23	-0.18	-0.35	0.37	0.16	-0.32	*0.77*
M_3	Cr	-1.34	0.03	-0.73	0.09	0.84	-0.33	*1.00*
	Fe	-0.98	0.33	-0.48	0.05	0.70	-0.52	0.67
	Co	-0.76	0.06	-0.56	0.16	0.52	-0.25	0.73
	Ni	-0.31	0.14	-0.71	0.66	0.31	-0.34	0.49
	Mo	-0.79	0.33	-0.57	0.32	0.37	-0.42	*1.07*
	W	-0.92	0.15	-0.60	0.28	0.31	-0.55	*1.14*

Table S9. DFT-calculated variation in spin magnetic moment (μ, μ_B) for adsorbates on $M_n@C_2N$ during the progress of HER and NRR.

		*	*H	side-on $*N_2$	side-on $*N_2H$	$*NH_2$	$*NH_3$
M_1	Fe	4.0	1.0	4.0	1.8	3.0	3.5
	Co	1.0	2.0	1.0	0.0	0.0	2.1
	Ni	2.0	1.0	0.0	0.8	1.0	1.8
	Cr	4.0	3.0	/	/	/	/
	Mo	2.0	1.0	2.0	1.0	1.0	2.0
	W	2.0	1.0	2.0	0.4	1.0	2.0
M_2	Fe	4.0	2.0	2.0	3.0	3.0	4.0
	Co	2.0	0.0	0.0	1.0	1.0	0.9
	Ni	0.0	1.0	2.0	0.0	0.5	1.5
	Cr	2.0	0.0	0.0	1.0	5.0	4.0
	Mo	0.0	2.0	0.0	0.9	1.0	0.0
	W	0.0	0.0	0.0	0.0	1.0	0.0

| M$_3$						
Fe	6.0	7.0	6.0	4.9	9.0	5.8
Co	3.0	3.0	3.0	0.0	3.0	1.0
Ni	0.0	0.0	0.0	0.5	0.5	1.7
Cr	4.0	3.0	4.0	3.0	3.0	2.0
Mo	0.0	0.0	0.0	1.0	0.3	0.0
W	0.0	0.0	0.0	1.0	0.3	0.0
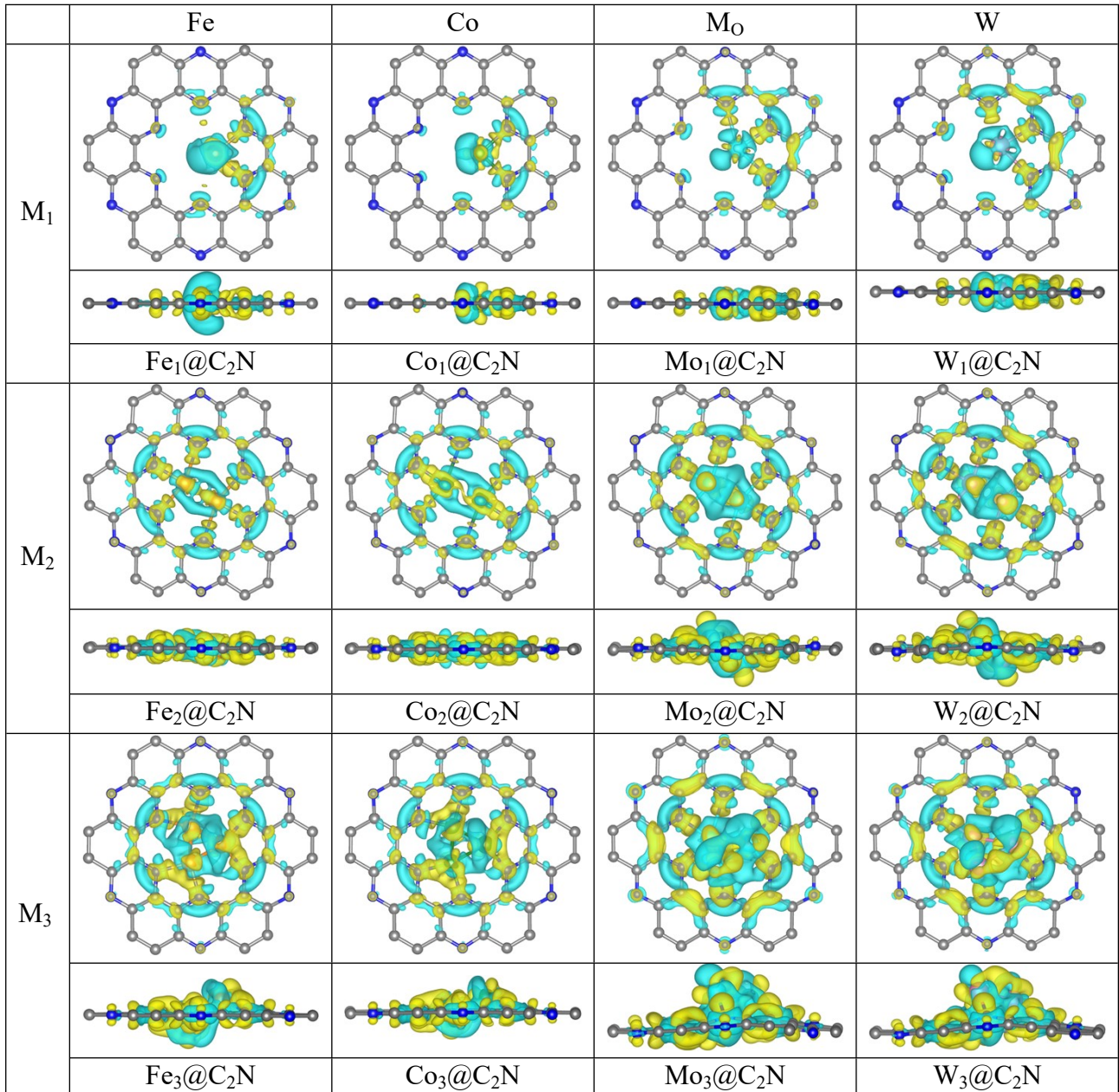
Figure S1. The differential charge diagram of M$_n$@C$_2$N along with isosurface of charge density difference ($\Delta\rho$), where $\Delta\rho = \rho_{(Mn@C2N)} - \rho_{(C2N)} - \rho_{(Mn)}$, and isosurface level=0.004 e/Bohr^3. Yellow: charge accumulation; Cyan: charge depletion.
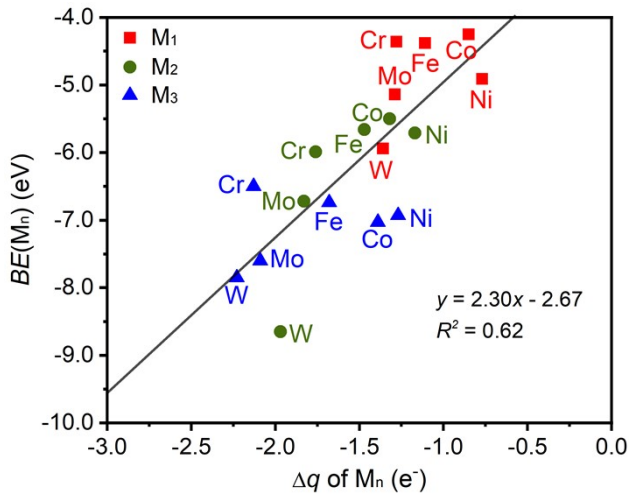
Figure S2. Linear trend of charge transfer (Δq) and binding energy (*BE*) of M_n.
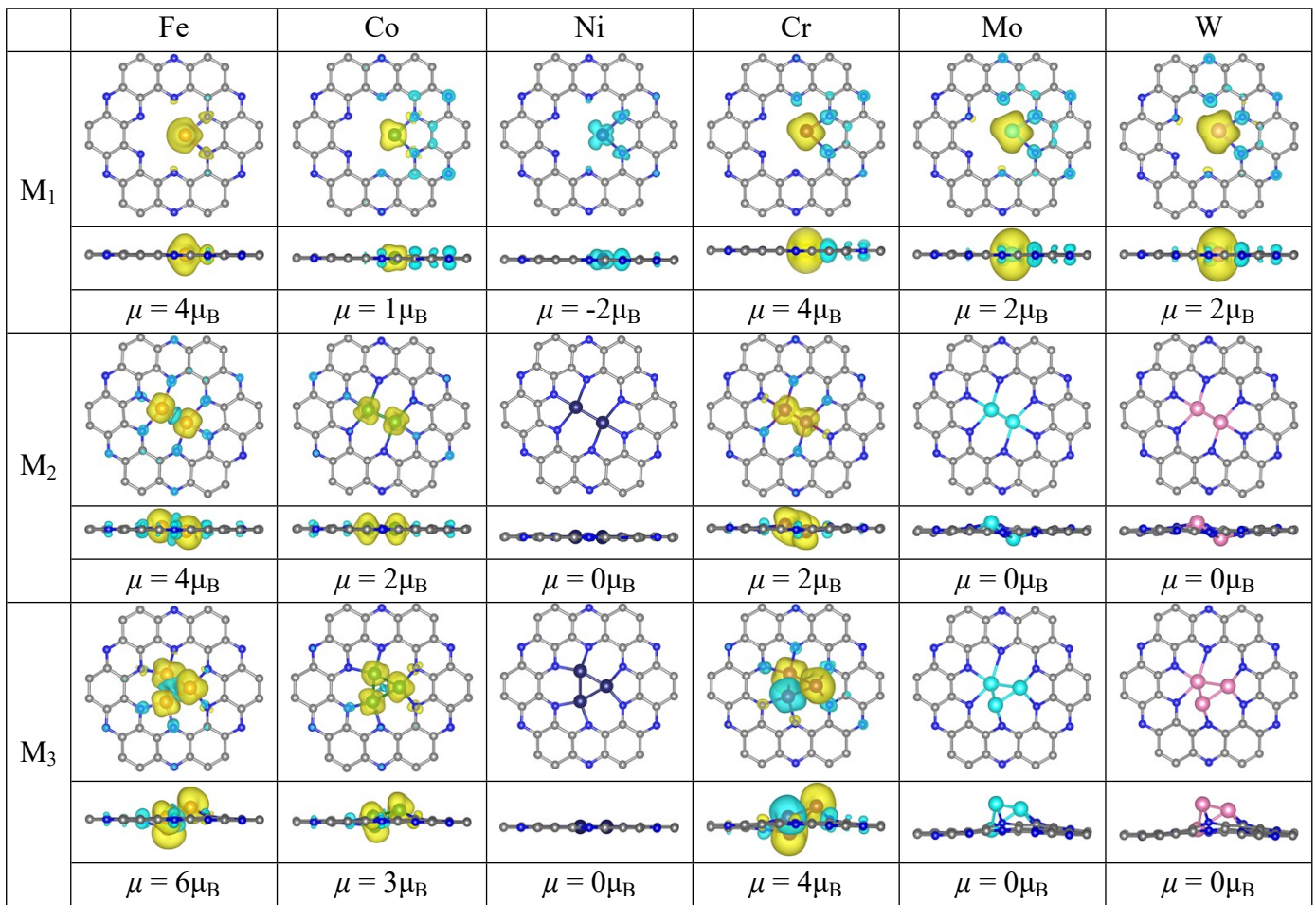
Figure S3. Net spin density for $M_n@C_2N$ (M = Fe, Co, Ni, Cr, Mo and W) at the isosurface level of $0.004\ e/Bohr^3$.
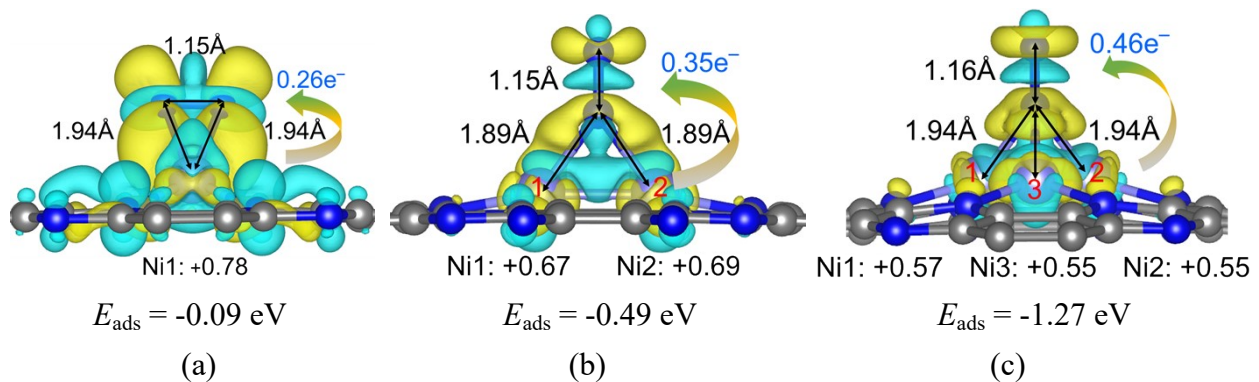
**Figure S4.** Isosurface of charge density difference for N_2 binding on $M_n@C_2N$ (a) $Ni_1@C_2N$, (b) $Ni_2@C_2N$, (c) $Ni_3@C_2N$ in side-on or end-on configuration. The corresponding bond length and the charge transferred to adsorbed N_2 are labeled. Isosurface level=0.004 e/Bohr^3. Yellow: charge accumulation; Cyan: charge depletion.
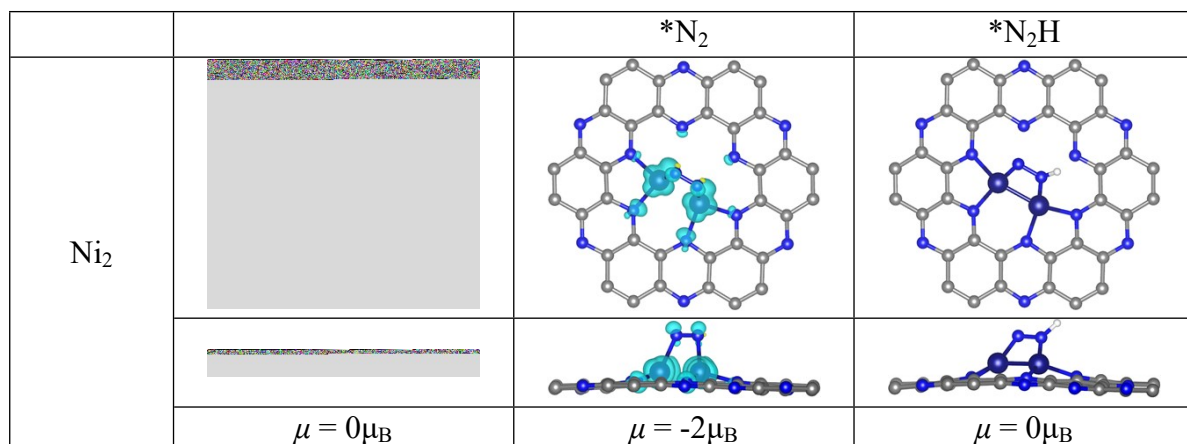
		*N_2	*N_2H
Ni_2			
	$\mu = 0\mu_B$	$\mu = -2\mu_B$	$\mu = 0\mu_B$

Figure S5. Net spin density for $Ni_2@C_2N$ (*N_2 and *N_2H) at the isosurface level of 0.004 e/Bohr^3.

	*N$_2$	*N$_2$H	*NH$_2$	*NH$_3$
N$_1$Fe$_1$N$_1$				
N$_1$Co$_1$N$_1$				
N$_1$Ni$_1$N$_1$				
N$_1$Mo$_1$N$_1$				
N$_1$W$_1$N$_1$				
N$_3$Fe$_2$N$_3$				
N$_3$Co$_2$N$_3$				
N$_2$Ni$_2$N$_2$				
N$_3$Cr$_2$N$_3$				
N$_3$Mo$_2$N$_3$				
N$_3$W$_2$N$_3$				
N$_2$Fe$_3$N$_2$				
N$_2$Co$_3$N$_2$				
N$_2$Ni$_3$N$_2$				
N$_2$Cr$_3$N$_2$				
N$_3$MoN$_2$MoN$_1$Mo				
N$_3$WN$_2$WN$_1$W				
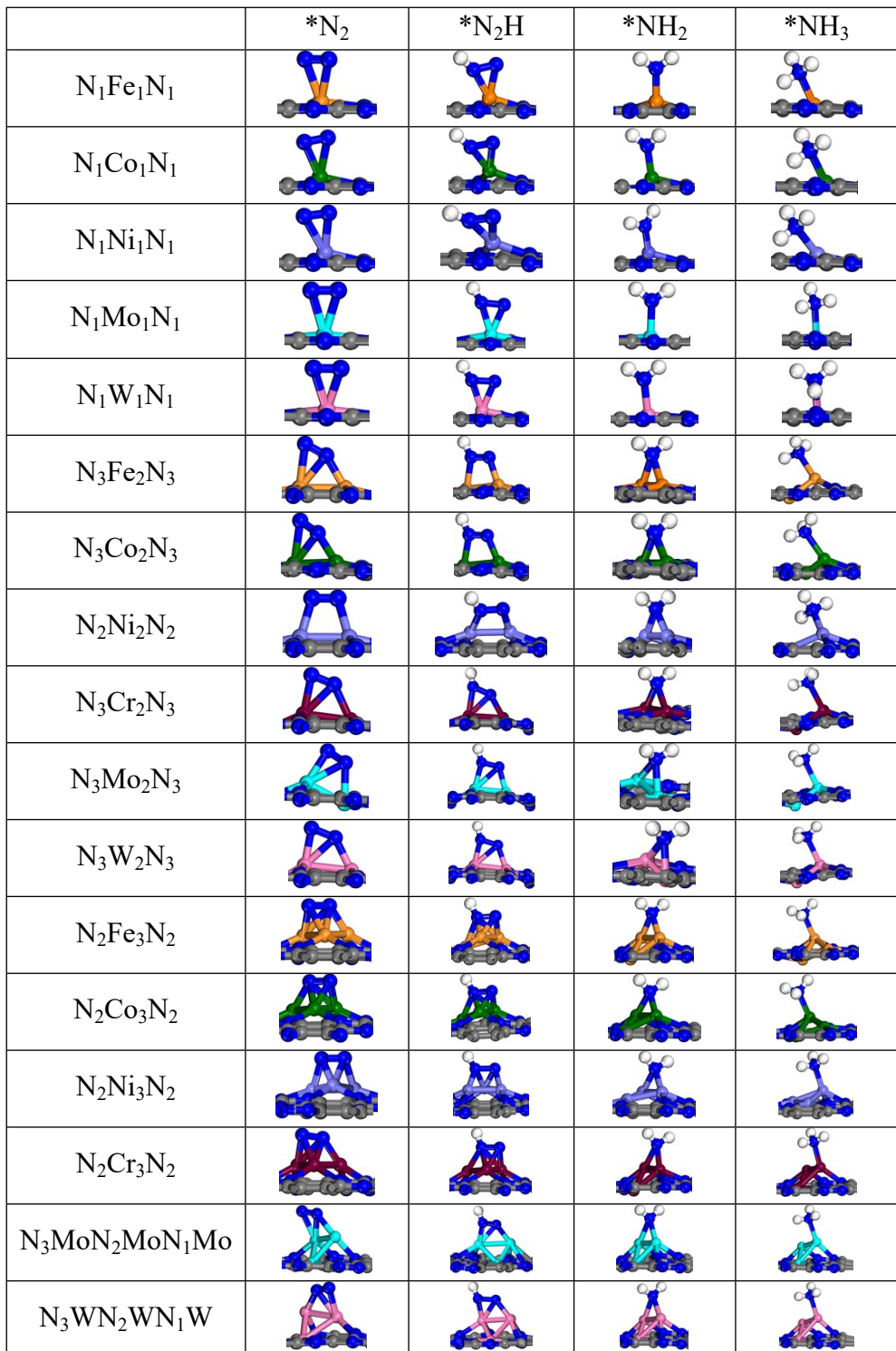
Figure S6. DFT-optimized structures of *N$_2$, *N$_2$H, *NH$_2$ and *NH$_3$ on M$_n$@C$_2$N.
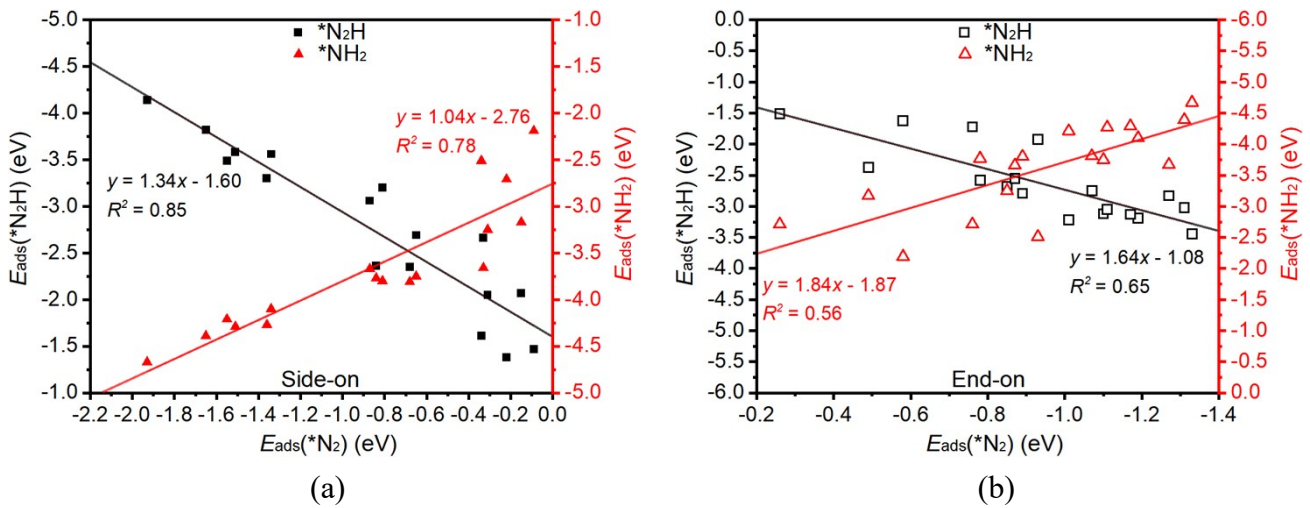
Figure S7. Scaling relations for adsorption energy (E_{ads}) of *N$_2$H/*N$_2$ and *NH$_2$/*N$_2$ for (a) side-on and (b) end-on mode of *N$_2$, where E_{ads} is referenced to gaseous N$_2$, N$_2$H and NH$_2$ for absolute binding strength.
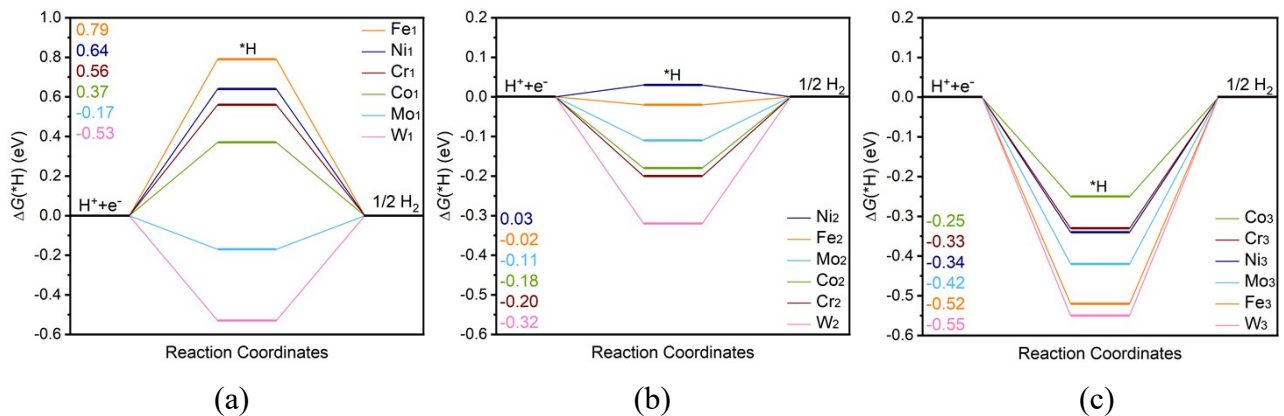

Figure S8. Gibbs free energy diagrams for Volmer-Heyrovsky mechanism of HER on M$_n$@C$_2$N at 0 V (vs. RHE). The full coverage of *H was employed to calculate *H binding on M$_n$@C$_2$N whose largest E_{ads} was chosen for HER (Figure S9).
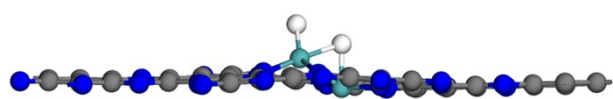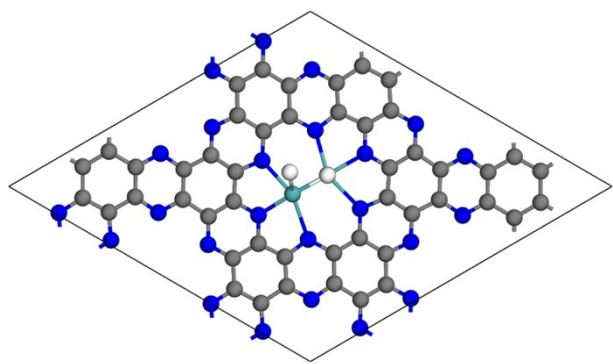
$E_{ads} = \textbf{-0.66}$ eV

(a)
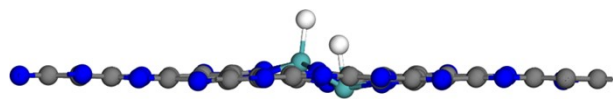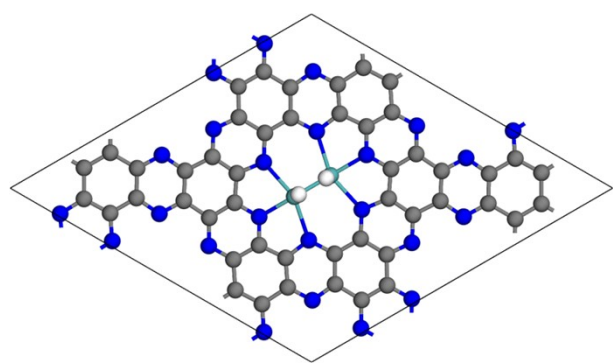
$E_{ads} = -0.36$ eV

(b)
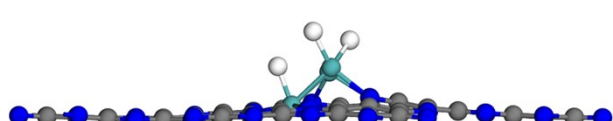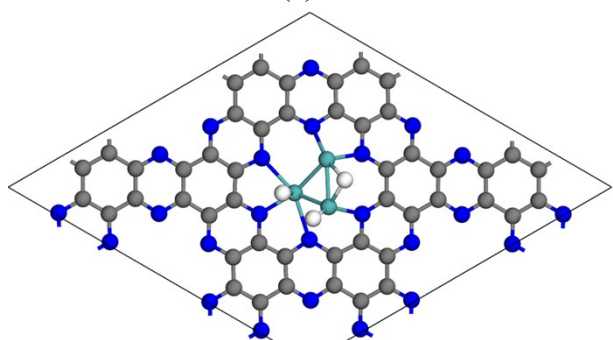
$E_{ads} = -1.97$ eV

(c)
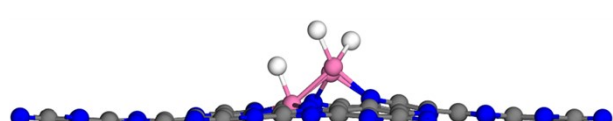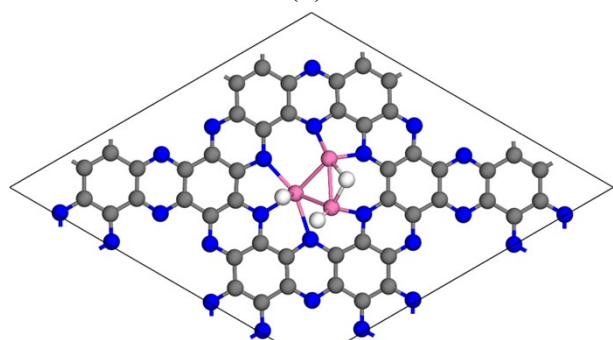
$E_{ads} = \textbf{-2.35}$ eV

(d)

Figure S9. Adsorption configurations of full coverage of *H on (a) $Mo_2@C_2N$, (b) $Mo_2@C_2N$, (c) $Mo_3@C_2N$, (d) $W_3@C_2N$.

1.   Wang, H.; Liu, Z., Comprehensive Mechanism and Structure-Sensitivity of Ethanol Oxidation on Platinum: New Transition-State Searching Method for Resolving the Complex Reaction Network. *J. Am. Chem. Soc.* **2008**, *130*, 10996-11004.